Applied Catalysis B: Environmental 164 (2015) 488–495

Contents lists available at ScienceDirect

Applied Catalysis B: Environmental

journal homepage: www.elsevier.com/locate/apcatb

Review

Nanosized IrOx and IrRuOx electrocatalysts for the O_2 evolution reaction in PEM water electrolysers

S. Siracusano[a,*], N. Van Dijk[b], E. Payne-Johnson[b], V. Baglio[a], A.S. Aricò[a]

[a] CNR-ITAE, Istituto di Tecnologie Avanzate per l'Energia "Nicola Giordano", Via Salita S. Lucia sopra Contesse 5, 98126 Messina, Italy
[b] ITM Power (Research) Ltd, Unit H, Sheffield Airport Business Park, Europa Link, Sheffield S9 1XU, United Kingdom

ARTICLE INFO

Article history:
Received 25 June 2014
Received in revised form 1 September 2014
Accepted 4 September 2014
Available online 16 September 2014

Keywords:
PEM electrolyser
Oxygen evolution reaction
Water electrolysis
Iridium ruthenium oxide electrocatalyst

ABSTRACT

IrOx and $Ir_{0.7}Ru_{0.3}Ox$ nanosized materials of similar crystallite size (5 nm) were prepared for application as oxygen evolution electrocatalysts in solid polymer membrane water electrolysers (PEMWEs). The physico-chemical properties of the catalysts were characterized by X-ray diffraction (XRD), Transmission Electron Microscopy (TEM), Scanning Electron Microscopy (SEM) with Energy Dispersive X-ray (EDX) and X-ray-Photoelectron Spectroscopy (XPS). Particular efforts were addressed to tailor the crystallographic characteristics and the surface properties. The electrochemical properties were investigated in an electrolysis cell, based on Nafion 115 and 30% Pt/C as cathode catalyst, by using linear sweep voltammetry, electrochemical impedance spectroscopy and Tafel curves. The $Ir_{0.7}Ru_{0.3}Ox$-based electrocatalyst showed a performance of 3.2 A cm^{-2} at 1.85 V at 90 °C which corresponds to a voltage gain of 0.1 V as compared to the IrOx catalyst at the same current density. Alternatively, an increase in current density of 0.6 A cm^{-2} is achieved at 90 °C and 1.85 V for the IrRuOx anode. A similar Tafel slope with a decrease of charge transfer resistance for IrRuOx compared to IrOx would indicate the same mechanism for these materials and higher intrinsic activity for the mixed oxide.

Contents

1. Introduction

Today the majority of hydrogen production comes from non-electrochemical processes such as reforming of natural gas and refinery gas (48%); hydrogen is a by-product in several production processes of chemicals (30%); it is also obtained from coal gasification (18%) [1–4]. Only 4% of the global hydrogen production comes from electrolysis, although originally hydrogen was produced almost exclusively by this way. Recently, interest in water electrolysis has increased again with the increasing diffusion of renewable energy sources and the perspective to produce hydrogen with a very low environmental impact [5–7].

Four different types of electrolysis technologies are currently available namely conventional Alkaline electrolysers (liquid electrolyte) [8–10], Proton Exchange Membrane (PEM) electrolysers [11–17], high temperature Solid Oxide electrolysers [18,19] and most recently Anion Exchange Membrane (AEM) electrolysers [20–22]. Historically, alkaline electrolysis has dominated the

* Corresponding author. Tel.: +39 090 624241; fax: +39 090 624247.
E-mail address: siracusano@itae.cnr.it (S. Siracusano).

http://dx.doi.org/10.1016/j.apcatb.2014.09.005
0926-3373/

market. This is considered a mature technology. PEM electrolysis has been commercially available for about 10 years. Solid oxide electrolysis has the promise for cost reduction. The solid oxide system, which operates at high temperature, could produce hydrogen with much lower electricity input than conventional electrolysers provided that waste heat is supplied to sustain the endothermic process. Whereas AEM technology has appeared on the market only very recently.

PEM electrolysis typically requires expensive materials to achieve lifetimes and efficiencies superior to the mature alkaline technology but at the same time offers advantages in terms of high degree of gas purity, high current density, higher safety level deriving from the use of a solid polymer electrolyte separator and high working pressure [11–13,23–25]. To reduce capital costs of PEM electrolysers, a higher production capacity at the same or better efficiencies than alkaline systems is needed. Therefore, most of PEM electrolysis activity is focused on materials and component development.

Noble metal materials, typically iridium and ruthenium oxides, are currently used as catalysts for the oxygen evolution reaction (OER) to provide high corrosion resistance and good catalytic activity. While the ruthenium oxide generally shows a higher activity, the iridium oxide has a better long-term stability [17,26].

In principle, there are many useful methods available for the synthesis of noble metal based oxides [27–30]. The polyol method is a relatively simple way to synthesize nanosized noble metal colloids of iridium or ruthenium [31,32] by the reduction of metal precursors in ethylene glycol. These metallic materials can then be thermally treated in air to form the oxide materials. Sol–gel methods have also proved useful in producing noble metal based oxides [33–37]. A modified polyol method in which a glycol-precursor solution is heated under nitrogen atmosphere to the refluxing temperature to obtain a colloid was proposed by Marshall et al. [38]. The Adams fusion method [39] has been widely used to produce fine noble metal oxide powders [40–44]; it is based on the oxidation of metal precursors in a molten sodium nitrate melt. One drawback associated to this procedure is often the occurrence of sodium impurities that can affect the electrocatalytic behaviour.

In this work, the oxygen evolution behaviour of iridium oxide and iridium–ruthenium oxide prepared by the Adams fusion synthesis using the procedure modified by Marshall but introducing a final step of catalyst pre-leaching has been investigated. The electrocatalysts have been evaluated in a single cell polymer electrolyte water electrolyser by linear sweep voltammetry, electrochemical impedance spectroscopy and Tafel slope.

Beside chemistry aspects, the electrochemical performance of an oxygen evolution electrocatalysts is related to the morphology, crystallographic characteristics and surface properties. In this regard, the properties of these electrocatalysts have been studied by using both ex situ physico-chemical characterization and in situ electrochemical methods. As well known, the electrolysis process occurs on the electrocatalysis surface at the interface with the electrolyte. Accordingly, the oxidation state of the elements in the outermost layers and the occurrence of impurities on the surface may affect the comparison of different catalyst formulations. Despite these evidences, there are not many reports providing a complete data-set of the catalysts characteristics including surface properties. In this work, efforts have been focused on the comparison of catalysts with similar crystallite size, same crystallographic structure and oxidation state on the surface, for the common element, and characterized by the absence of impurities such as Na, S, Cl, Si, etc. Previous reports and comparisons in the literature, dealing with this type of electrocatalyst formulations, have often regarded materials characterized by different particle size, morphology, oxidation states, etc. where it was difficult to discriminate the effect of each variable on the electrokinetic properties. Whereas, the aim of this work is to provide a performance comparison between two catalyst chemistries while minimizing the effect of other variables and to understand the effect of the different chemistry on the electrokinetic properties for oxygen evolution.

2. Experimental

2.1. Synthesis of electrocatalysts

Both IrOx and IrRuOx electrocatalysts were synthesized by the Adams fusion method using the procedure modified by Marshall [38]. The metal precursors ($IrCl_4{\cdot}xH_2O$ or $RuCl_3{\cdot}xH_2O$, Strem Chemicals) were added to isopropanol to obtain a total metal concentration of 0.08 M. This solution was magnetically stirred at room temperature for 1 h to ensure complete dissolution of the precursors, followed by the addition of $NaNO_3$, previously ground. The slurry was heated at 90 °C in air until completely dry. The dry salt was then placed in a furnace at 500 °C for 30 min. The fused salt-oxide was washed with distilled water to remove the remaining salts, filtered and dried in an oven at 80 °C for all night. To completely remove the sodium impurities, a pre-leaching procedure in $HClO_4$ (0.1 M, 80 °C, 1 h) was adopted in the present case.

The resulting powders were characterized by XRD, TEM, SEM-EDX and XPS. These analyses allowed to get information on crystallographic structure, morphology, bulk composition and composition of the outermost surface layers for the two different catalysts.

2.2. Physico-chemical characterization

XRD analysis was performed on the final catalyst powders by a Philips X-Pert diffractometer equipped with a CuKα as radiation source. This diffractometer operated at 40 kV and 20 mA, with a scan rate of 0.5 2θ min^{-1} and angular resolution of 0.005° 2θ. The diffraction patterns were fitted to Joint Committee on Powder Diffraction Standards (JCPDS). Rietveld refinement was used in order to reduce the error in evaluating the reflection peak position. To confirm the occurrence of a solid solution, catalysts with varying Ir/Ru atomic ratio were investigated. However, excluding this aspect, all remaining study was focused on the $Ir_{0.7}Ru_{0.3}Ox$ anode formulation that guarantees for proper stability in the electrolysis environment [15].

The morphology of the IrOx and $Ir_{0.7}Ru_{0.3}Ox$ catalysts was investigated by TEM. The specimen was prepared by ultrasonic dispersion of the catalyst in isopropyl alcohol and subsequently depositing a drop of the suspension on a carbon film-coated Cu grid. The analysis was carried out with a FEI CM12 microscope.

Scanning Electron Microscopy (SEM) with Energy Dispersive X-Ray (EDX) analysis was carried out by a FEI XL30 SFEG microscope. The instrument was operated at 25 kV and the EDX probe was used to determine the bulk elemental composition of the samples.

The surface chemical composition of the catalysts was investigated by XPS using a Physical Electronics (PHI) 5800-01 spectrometer. A monochromatic Al Ka X-ray source was used at a power of 300 W. Spectra were obtained with a pass energy of 58.7 eV for elemental analysis (composition) and 11.75 eV for the determination of the chemical species. The pressure in the analysis chamber of the spectrometer was 1×10^{-9} Torr during the measurements. Spectra were collected at a photo-electron take-off angle of 45° with respect to the sample surface.

2.3. Preparation of the membrane-electrode assembly (MEA)

IrOx and $Ir_{0.7}Ru_{0.3}Ox$ were used as anodic catalysts. A slurry composed of 80 wt.% catalyst and 20 wt.% Nafion ionomer (5 wt.% Ion Power solution) in deionised water and anhydrous Ethanolic

alcohol (Carlo Erba) was prepared by mixing under ultrasounds. The slurry was directly deposited onto one face of the membrane (Nafion 115) by using a spray coating technique. The anode catalyst loading was 1.5 mg cm^{-2}. A Ti fibre (Bekaert Toko Metal Fiber Co.), 300 μm thick characterized by about 70% porosity, was used as backing layer for the anode side. A 30% Pt/Vulcan XC-72 prepared as described in Ref. [45] was used as the catalyst for the H_2 evolution. The cathode catalyst was spread on carbon cloth backing (GDL ELAT from ETEK, 300 μm thick carbon cloth with carbon black loading of about 5 mg cm^{-2} and 30% PTFE content) with a Pt loading of 0.5 mg cm^{-2}. The ionomer content in the cathode layer was 33 wt.% after drying. Membrane-electrode assemblies (MEAs), with 5 cm^2 geometrical area, were prepared by a hot-pressing procedure. Specifically, the cathode was hot pressed onto one face of the Nafion 115 membrane, already coated with the electrocatalyst on the anode side, at 130 °C for 1.5 min. Two PTFE sheets were used to avoid direct contact of the MEA components with the heating plates.

2.4. Electrochemical characterization

The 5 cm^2 PEM single cell electrolyser performance was evaluated at different temperatures and under atmospheric pressure. Deionised water was pre-heated at the same cell temperature and supplied by a pump, at a flow rate of 4 ml min^{-1}, to the anode compartment. Polarization curves (cell potential as a function of current density) and electrochemical impedance spectroscopy (EIS) were carried out by a PGSTAT Autolab 302 Potentiostat/Galvanostat equipped with a booster of 20 A (Metrohm) and a Frequency Response Analyser (FRA). The EIS measurements were performed under potentiostatic control in a frequency range between 20 kHz and 0.1 Hz by frequency sweeping in the single sine mode. The amplitude of the sinusoidal excitation signal was 0.01 V r.m.s. The series resistance was determined from the high frequency intercept on the real axis in the Nyquist plot. The polarization resistance was taken as the difference between the extrapolated low frequency intercept and the high frequency intercept on the real axis.

Polarization results were highly reproducible (standard deviation within 0.5%). The reported results are the result of an average of at least three polarization data-set.

Hydrogen gas flows were measured at constant current density after having condensed all humidity present in the gas stream in order to determine the Faradaic efficiency.

3. Results and discussion

Fig. 1a shows the XRD patterns of the IrOx and $Ir_{0.7}Ru_{0.3}Ox$ catalysts. A tetragonal crystallographic structure typical of IrO_2 is observed for both samples. As IrO_2 and RuO_2 have identical structure with very similar magnitude lattice parameters and the ionic radii of the iridium and ruthenium are very similar, it is believed these metals oxides can exist in solid solution. Indeed a shift towards higher Bragg angles with respect to the reference IrO_2 (JCPDS card no. 15870) is observed in the XRD pattern of the $Ir_{0.7}Ru_{0.3}Ox$ catalyst (see inset of Fig. 1a); this indicates a lattice contraction suggestive of the formation of a solid solution. The crystallite sizes, determined by the Debye–Scherrer equation, were 5.3 and 5 nm for IrOx and $Ir_{0.7}Ru_{0.3}Ox$, respectively.

Fig. 1b shows this lattice contraction continues along one dimension, lattice parameter *c*, with increasing ruthenium content. It can be observed that lattice parameter *a* is almost identical (within 0.008 Å) for synthesized IrOx, RuOx and their intermediates as anticipated from the reference IrO_2 and RuO_2 (JCPDS cards no. 15870 and 21-1172). The small magnitude of changes in the lattice contraction necessitated the use of Rietveld refinement in order to reduce the error in evaluating the reflection peak position. The variation of lattice parameter *c* with concentration of ruthenium is indicative of the attainment of a solid solution.

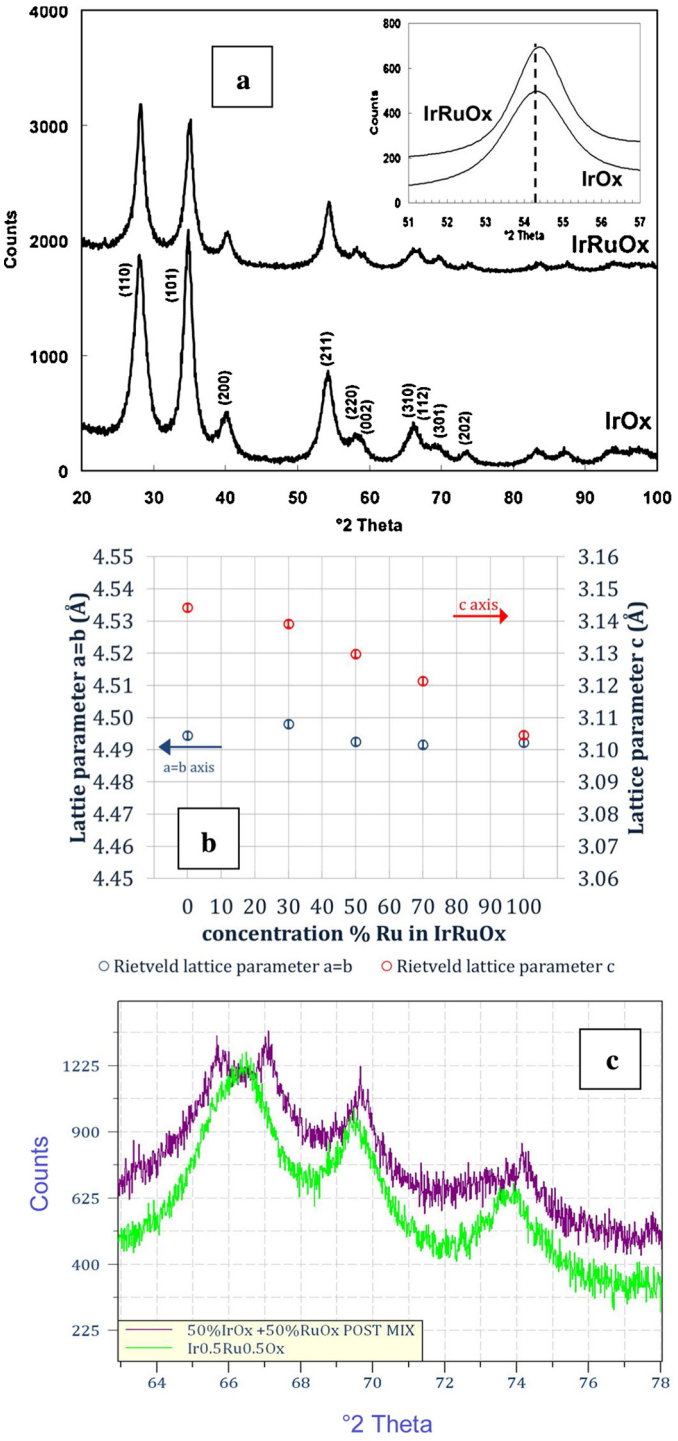

Fig. 1. (a) XRD patterns of the IrOx and $Ir_{0.7}Ru_{0.3}Ox$ catalysts; (b) crystallographic parameters for IrRuOx as a function of Ru content; (c) comparison of mechanically mixed IrOx and RuOx with the synthesized solid solution at the equimolar Ir/Ru ratio.

Confirmation of successful solid solution formation is shown in Fig. 1c, where $Ir_{0.5}Ru_{0.5}Ox$ has been compared directly to a mixed material made using synthesized IrOx and RuOx mixed in the same molar ratios. It can be observed that the ruthenium oxide (112) reflection is absent in the solid solution.

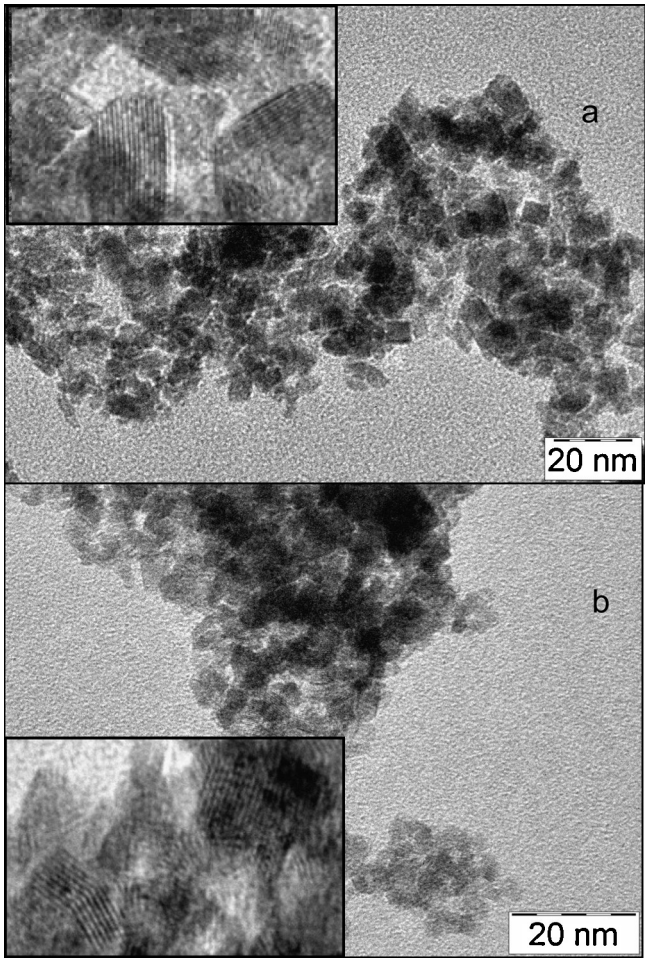

Fig. 2. TEM micrographs of IrOx (a) and $Ir_{0.7}Ru_{0.3}Ox$ (b) catalysts.

This analysis was essentially carried out just to provide a clear evidence of the formation of a solid solution for a catalysts characterized by an equimolar ratio of Ir and Ru to corroborate the evidence of solid solution for the $Ir_{0.7}Ru_{0.3}Ox$ formulation. It is well known that a large content of Ru can decrease the catalysts stability [15]. Thus, our efforts in this work were focused on the $Ir_{0.7}Ru_{0.3}Ox$ formulation.

The morphology of these catalysts were investigated by TEM. A TEM image of the IrOx catalyst reported in Fig. 2a shows the presence of agglomerates composed of fine particles. Interesting, several particles show a rectangular shape on the TEM imaging. Thus, a significant fraction of these particles are faceted than round (spherical). The inset shows the crystalline fringes of the primary IrO_2 particles. In Fig. 2b, the micrograph of the $Ir_{0.7}Ru_{0.3}Ox$ catalyst is shown. Also in this case, there is the presence of agglomerates composed of fine particles. The lattice fringes were used to estimate the mean size of the crystalline domains for both catalysts. These were about 5.4 nm and 5.2 nm for IrOx and $Ir_{0.7}Ru_{0.3}Ox$, respectively, in good agreement with XRD line broadening.

A comparison of two EDX spectra for IrOx and $Ir_{0.7}Ru_{0.3}Ox$ catalysts obtained at low magnification (150×) is reported in Fig. 3. The EDX analysis was utilized to investigate elemental bulk composition. This was Ir:Ru = 70:30 in agreement with the nominal one.

The surface analysis was carried out by XPS. A comparison of the survey spectra for the two catalysts is shown in Fig. 4. By comparing the photoelectron lines for the two samples, it clearly appears that no impurities are present on the surface. High-resolution spectra for the two catalysts are shown in Fig. 5. The Ir4f photoelectron

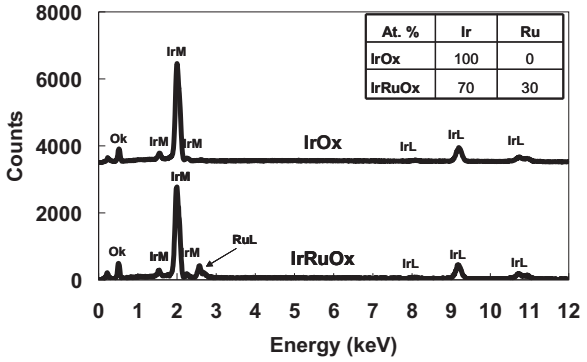

Fig. 3. SEM-EDX of the IrOx and $Ir_{0.7}Ru_{0.3}Ox$ catalysts.

lines appeared at the same B.E. of 61.8 and 64.8 for both samples (Fig. 5a) indicating the prevailing occurrence of Ir^{3+} oxidation state on the surface. Whereas, in the case of $Ir_{0.7}Ru_{0.3}Ox$, the Ru3p3/2 photoelectron line occurred at 462.8 B.E (Fig. 5b) that can be associated to the presence of Ru^{4+} species on the surface. These different oxidation states for Ir and Ru in the outermost layers can promote the electron transfer at the interface through a redox mechanism [46,47]. The surface atomic composition as determined by the XPS analysis was Ir:Ru = 75:25 for the IrRuOx catalyst indicating a slight segregation of Ir on the surface. Whereas after sputtering with Ar^+ ions at 5 kV for 30 min (not shown), the atomic composition of the mixed oxide catalyst was Ir:Ru = 70:30 in good agreement with the nominal one. The surface enrichment in Iridium versus bulk composition has been probably promoted by pre-leaching treatment in perchloric acid. However, surface segregation of IrOx was also observed in RuO_2–IrO_2 mixed oxide layers prepared by thermal decomposition [46–48], and catalyst prepared hydrothermally [49]. It has been observed that XPS analysis can provide limited information on the inner surface [48]; in our case, after a sputtering treatment, the XPS analysis provided a composition matching the nominal bulk composition. This is also in agreement with the depth-profiling studies carried out by De Battisti et al. [50].

Fig. 6 shows single cell polarization curves for the IrOx-based MEA in the range of temperature from 30 °C to 90 °C under atmospheric pressure. There is a progressive increase of performance with temperature. The best performance at high current densities for water electrolysis was obtained at 90 °C. The current density at

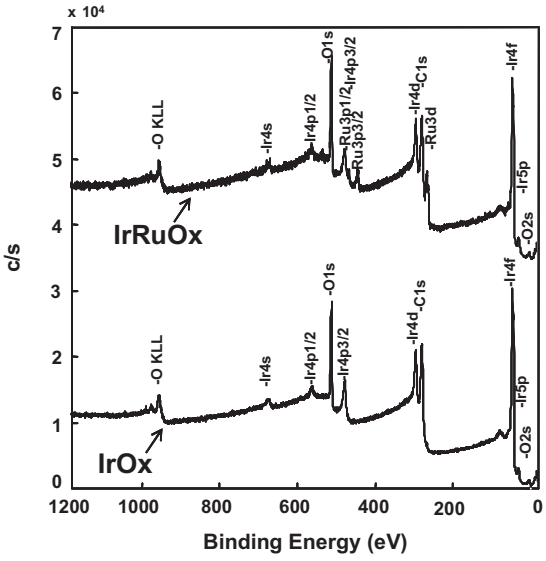

Fig. 4. XPS survey spectra of the IrOx and $Ir_{0.7}Ru_{0.3}Ox$ catalysts.

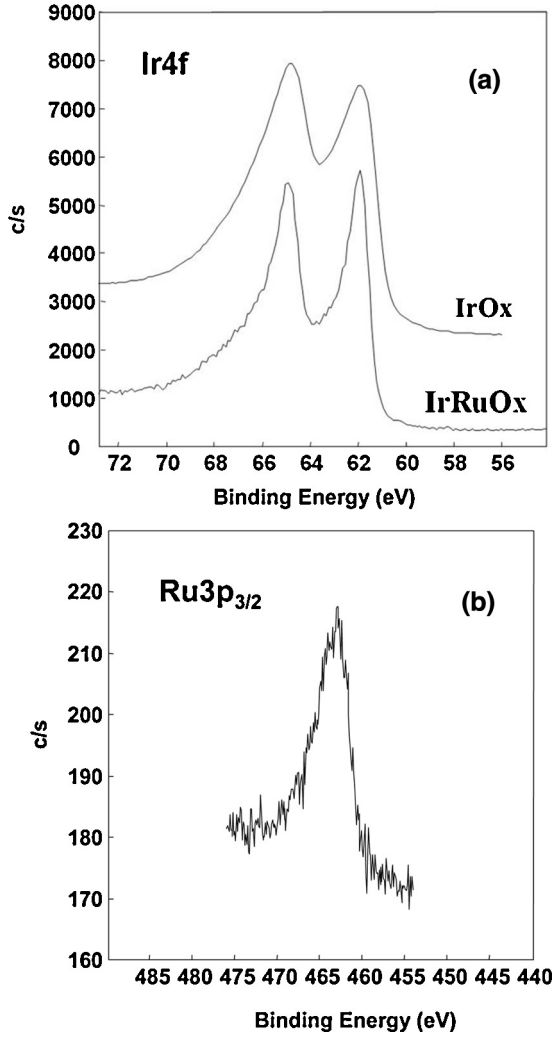

Fig. 5. XPS spectra of: (a) Ir4f in both IrOx and $Ir_{0.7}Ru_{0.3}Ox$ catalysts; (b) Ru3p3 in Ir0.7Ru0.3Ox catalyst.

1.8 V and 90 °C was 2.1 A cm^{-2}. The impedance behaviour for this cell was evaluated at 1.5 V, being this potential slightly above the thermoneutral potential, and at different temperatures (Fig. 7). The series resistance (R_s) was determined from the intercept on the real axis of the Nyquist plot in the high frequency range. The polarization resistance (R_p) was obtained by the difference between the low and high frequency intercepts. Both series and polarization

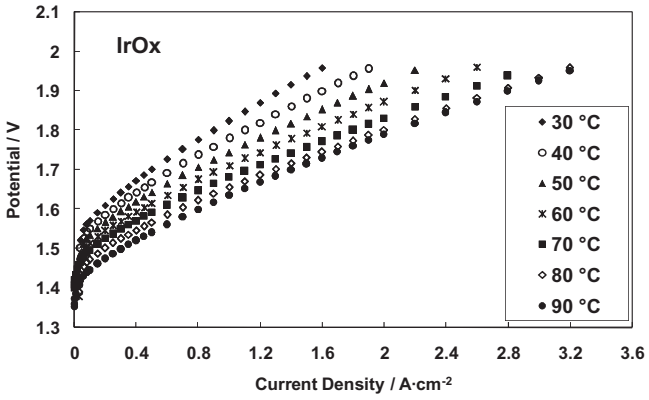

Fig. 6. Polarization curves of IrOx-based electrolyser cell at different temperature.

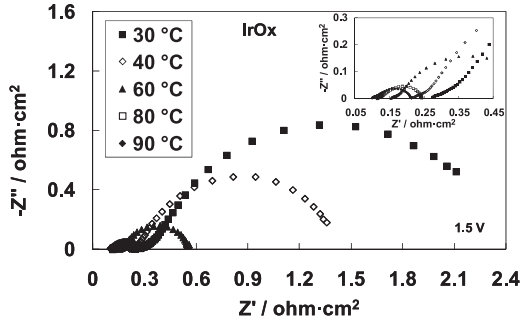

Fig. 7. Nyquist plots of IrOx-based electrolyser cell at 1.5 V and different temperatures.

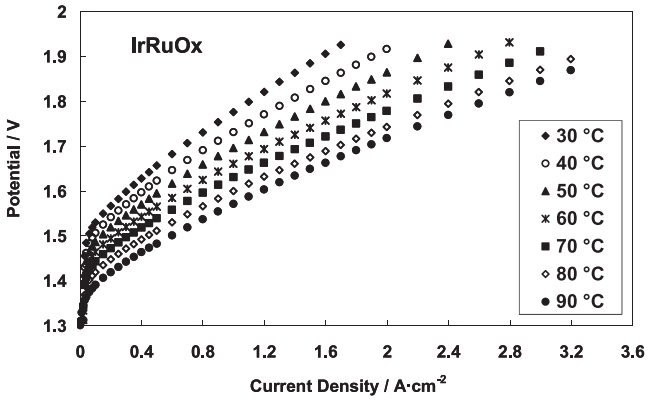

Fig. 8. Polarization curves of $Ir_{0.7}Ru_{0.3}Ox$-based electrolyser cell at different temperatures.

resistances decreased as the temperature increased. The lower R_s and R_p values were recorded at 90 °C i.e. 99 mΩ cm^2 and 113 mΩ cm^2, respectively.

The polarization curves at different temperatures under atmospheric pressure for the $Ir_{0.7}Ru_{0.3}Ox$-based MEA are shown in Fig. 8. Also in this case, the electro-catalytic activity increased as a function of temperature, reaching the best performance at 90 °C. A current density of 2.6 A cm^{-2} was recorded at 1.8 V and 90 °C. Faradaic efficiencies in excess of 99% were determined in the range of current densities of 0.5–2.5 A cm^{-2} at 90 °C by measuring hydrogen gas flows at the cathode outlet after having condensed all humidity present in the gas stream.

The impedance plots (Nyquist) obtained by the EIS analysis for the $Ir_{0.7}Ru_{0.3}Ox$-based cell are reported in Fig. 9. Also in this case, both R_s and R_p decreased as a function of the increase of the temperature. A 90 °C the values were 98 mΩ cm^2 and 72 mΩ cm^2 for the

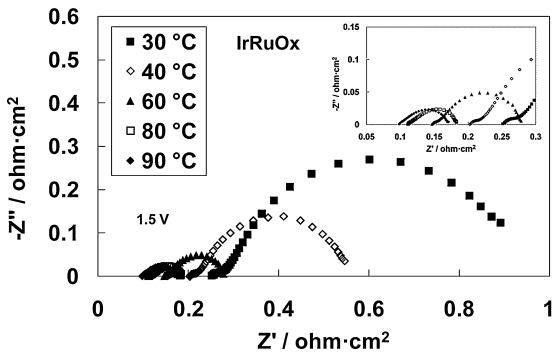

Fig. 9. Nyquist plots of $Ir_{0.7}Ru_{0.3}Ox$-based electrolyser cell at 1.5 V and different temperatures.

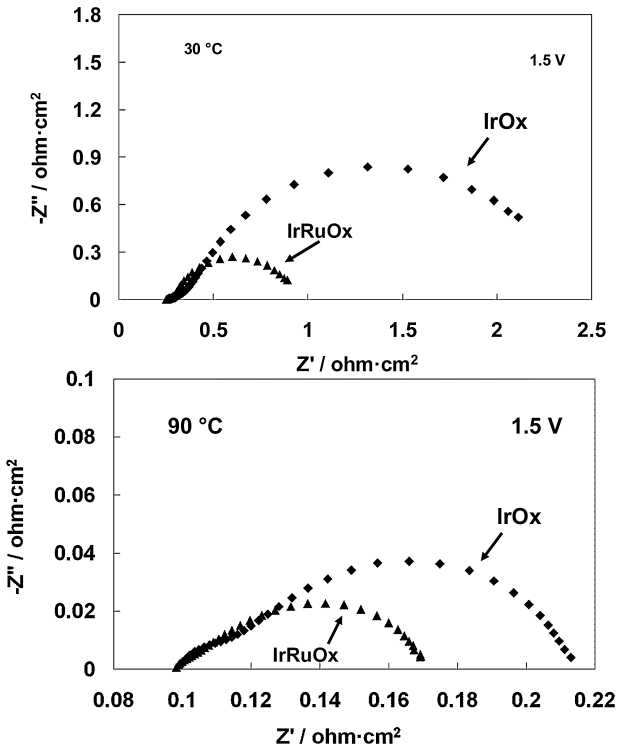

Fig. 10. Comparison of Nyquist plots of IrOx- and $Ir_{0.7}Ru_{0.3}Ox$-based electrolyser cells at 30 °C and 90 °C.

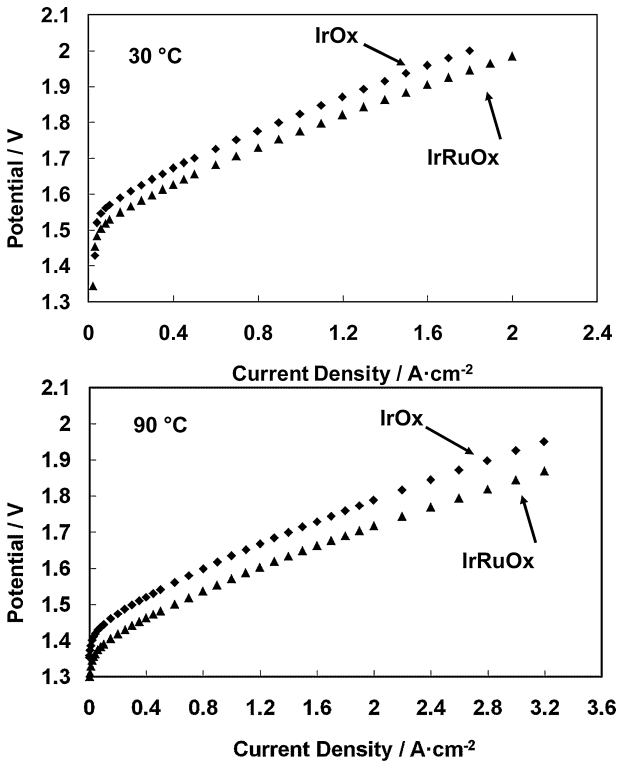

Fig. 11. Comparison of polarization curves of IrOx- and $Ir_{0.7}Ru_{0.3}Ox$-based electrolyser cells at 30 °C and 90 °C.

R_s and R_p, respectively. Thus, by comparing the impedance results, the IrOx and IrRuOx based MEAs show the same series (ohmic) resistance and different polarization resistances.

In Fig. 10 the impedance results for the IrO_2-based and $Ir_{0.7}Ru_{0.3}Ox$-based cells at 30 °C and 90 °C are shown. Similar R_s are recorded for both cells, whereas lower R_p are recorded at both temperatures for the $Ir_{0.7}Ru_{0.3}Ox$-based cell. This confirms that the presence of ruthenium in the catalyst improves the charge transfer for oxygen evolution in the electrolysis cell. Moreover a reduction in the anode catalyst cost by about 20% is envisaged.

At 90 °C, the polarization resistance of the IrRuOx catalyst is 63% of that recorded for the IrOx catalyst (Fig. 10). At 30 °C, the polarization resistance of the IrRuOx is 38% of that associated to IrOx. In fact at 30 °C R_p values are 2.11 Ω cm² and 0.6 Ω cm² for IrOx and IrRuOx, respectively (Fig. 10). These evidences indicate that the IrRuOx is better performing in the overall temperature range.

The polarization curves show an almost similar upperward shift in potential passing from IrRuOx to IrOx. Ohmic resistance becomes dominant at high current densities; however, the different activation behaviour of the two catalysts reflects on the entire polarization curves (Fig. 11).

Tafel curves in Figs. 12 and 13 show similar slopes for both catalyst in the range of 60–80 mV/dec. It should be considered that this Tafel slope also includes a small contribution of the hydrogen evolution electrode. A Tafel slope increasing from 40 to 60 mV dec^{-1} has been reported in the literature passing from RuO_2 to IrO_2 [51]. In our case, we have not observed significant changes probably on account of the fact that the amount of RuOx on the outermost layers is only 25%. However, Owe et al. [49] have also observed no large change of the Tafel slope with the composition. Most of these studies have been carried out at ambient temperature. The Tafel slope for the present catalysts slightly increases with temperature, in both cases, according to the Volmer–Butler equation [52]. Since the Tafel slope (symmetry of the activation barrier and number of electrons exchanged in the rate determining step) is similar for both

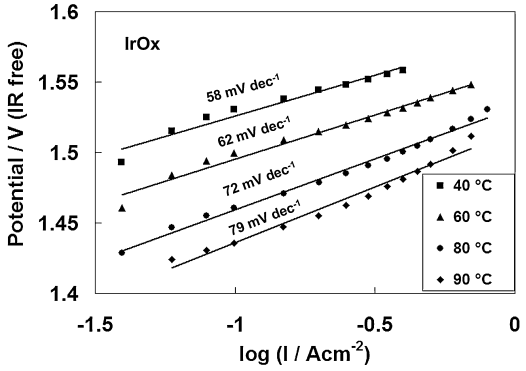

Fig. 12. Tafel plots for oxygen evolution reaction in IrOx-based electrolyser cell at different temperature.

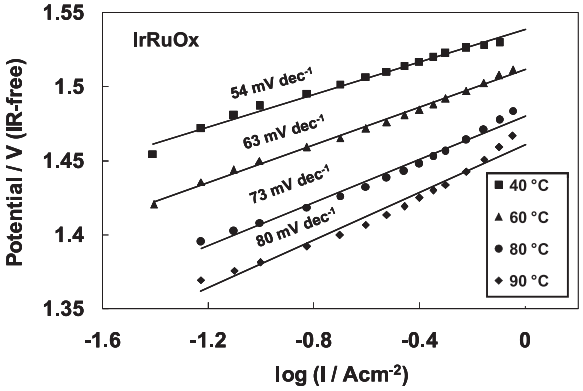

Fig. 13. Tafel plots for oxygen evolution reaction in $Ir_{0.7}Ru_{0.3}Ox$-based electrolyser cell at different temperature.

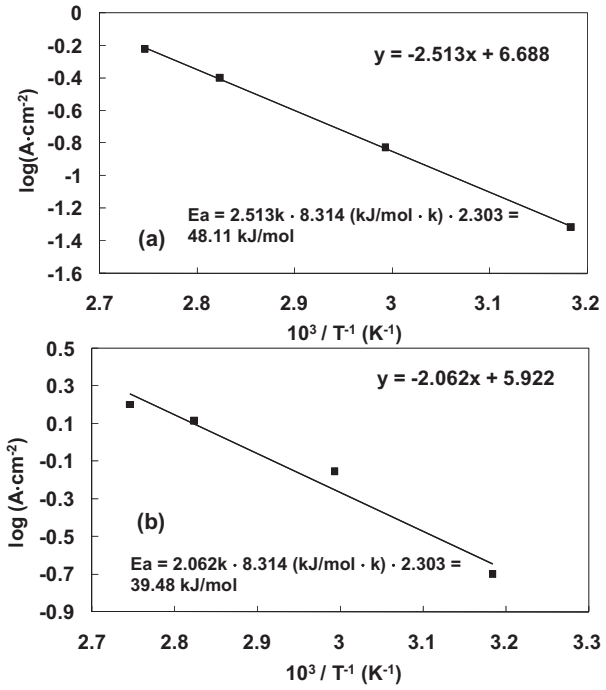

Fig. 14. Arrhenius plot of current density at 1.5 V as a function of temperature for the (a) IrOx- and (b) $Ir_{0.7}Ru_{0.3}Ox$-based electrolyser.

formulations, the current density measured at the same potential and under same conditions of temperature and pressure necessarily reflects the value of the reaction constant. The same Tafel slope for IrOx and IrRuOx would indicate a similar reaction mechanism; thus, being particle size, structure and morphology similar, the observed changes in current density reflect a different intrinsic catalytic activity (larger electrochemical rate constant for the IrRuOx) as consequence of the different chemistry.

The Arrhenius plots (Fig. 14) show an activation energy for the electrochemical process about 20% lower in the case of the mixed Ir–Ru oxide (39.5 kJ/mol) compared to IrOx (48.1 kJ/mol).

The reaction mechanism of O_2 evolution at Ir-based electrocatalysts has been investigated in the literature [53,54]. It is widely agreed that the reaction involves several steps e.g. water displacement on the surface, charge transfer and surface reaction of adsorbed intermediates to evolve molecular oxygen:

$$S + H_2O \rightarrow S{-}OHads + H^+ + e^-;$$

$$S{-}OHads \rightarrow S{-}Oads + H^+ + e^-;$$

$$S{-}Oads + S{-}Oads \rightarrow 2S + O_2$$

S represents an active sites on the catalyst surface e.g. Ir or Ru sites, and S—OHads, S—Oads are adsorption intermediates. The rate determining step depends on the strength of the adsorption of the reaction intermediates, which is in turn governed by the surface electronic properties of the electro-catalyst. In the present case, we have clearly observed a decrease of the activation energy for the mixed oxide catalyst that could be related to the ability of Ru species to promote water displacement at lower potentials [55].

The presence of the ruthenium in the electrocatalyst thus promotes the oxygen evolution reaction (OER) as reported in the literature [51,56]. However, RuO_2 is also known to be less stable than IrO_2. Thus, a solid solution with a moderate Ru content on the outercatalyst surface should represent a good compromise between activity and stability.

The performance achieved with the present IrRuOx catalyst appears comparable to the best state of the art reported in the literature for similar mixed oxide catalysts [44,57–61] despite a lower catalyst loading used in the present case. This is probably related to the high degree of purity of the present catalyst especially in the outermost surface layers.

Durability tests for the present IrRuOx catalyst at sustained current density in the presence of a perfluorosulfonic acid membrane are currently underway. According to the initial results, the recorded irreversible degradation appears moderate, in the range of several μV/h, and not significantly different than IrOx. The results will be reported in a next paper.

4. Conclusions

IrO_2-based and $Ir_{0.7}Ru_{0.3}Ox$-based electrocatalysts were prepared by a modified Adams fusion method. A pre-leaching procedure was applied to achieve high degree of surface purity and to promote an enrichment of Ir on the outer surface. The IrRuOx catalyst showed similar crystallographic properties, morphology and particle size of the IrOx catalyst. Also Tafel slope was similar indicating the occurrence of the same reaction mechanism; however, both polarization tests and ac-impedance spectra showed a better catalytic activity for the IrRuOx mixed oxide that is also reflected in a lower activation energy for the electrochemical process. The present study demonstrates that $Ir_{0.7}Ru_{0.3}Ox$-based electrocatalyst is an excellent catalyst for the oxygen evolution in PEM-based water electrolysis provided that structure, morphology and surface characteristics are properly modulated.

Acknowledgments

The authors acknowledge the financial support of the EU through the FCH JU ELECTROHYPEM Project. “The research leading to these results has received funding from the European Community’s Seventh Framework Programme (FP7/2010-2013) for the Fuel Cells and Hydrogen Joint Technology Initiative under grant agreement ELECTROHYPEM n. 300081.”

References

[1] H. Balat, E. Kirtay, Int. J. Hydrogen Energy 35 (2010) 7416–7426.
[2] C. Koroneos, A. Dompros, G. Roumbas, Chem. Eng. Process.: Process Intensif. 47 (2008) 1261–1268.
[3] D. Das, N. Khanna, T.N. Veziroglu, Chem. Ind. Chem. Eng. Q 14 (2008) 57–67.
[4] E. Kırtay, Energy Convers. Manage. 52 (2011) 1778–1789.
[5] O. Bičáková, P. Straka, Int. J. Hydrogen Energy 37 (2012) 11563–11578.
[6] J.D. Holladay, J. Hu, D.L. King, Y. Wang, Catal. Today 139 (2009) 244–260.
[7] A. Caravaca, A. de Lucas-Consuegra, A.B. Calcerrada, J. Lobato, J.L. Valverde, F. Dorado, Appl. Catal. B: Environ. 134–135 (2013) 302–309.
[8] L.M. Gandía, R. Oroz, A. Ursúa, P. Sanchis, P.M. Diéguez, Energy Fuels 21 (2007) 1699–1706.
[9] C.T. Bowen, H.J. Davis, B.F. Henshaw, R. Lachance, R.L. LeRoy, R. Renaud, Int. J. Hydrogen Energy 9 (1984) 59–66.
[10] L. Ma, S. Sui, Y. Zhai, Int. J. Hydrogen Energy 34 (2009) 678–684.
[11] S.P.S. Badwal, S. Giddey, F.T. Ciacchi, Ionics 12 (2006) 7–14.
[12] F. Barbir, Sol. Energy 78 (2005) 661–669.
[13] S.A. Grigoriev, V.I. Porembsky, V.N. Fateev, Int. J. Hydrogen Energy 31 (2006) 171–175.
[14] P. Millet, N. Mbemba, S.A. Grigoriev, V.N. Fateev, A. Aukauloo, C. Etiévant, Int. J. Hydrogen Energy 36 (2011) 4134–4142.
[15] M. Carmo, D.L. Fritz, J. Mergel, D. Stolten, Int. J. Hydrogen Energy 38 (2013) 4901–4934.
[16] A.S. Arico, S. Siracusano, N. Briguglio, V. Baglio, A. Blasi, V. Antonucci, J. Appl. Electrochem. 43 (2013) 107–118.
[17] A. Marshall, B. Børresen, G. Hagen, M. Tsypkin, R. Tunold, Energy 32 (2007) 431–436.
[18] M. Ni, M.K.H. Leung, D.Y.C. Leung, Int. J. Hydrogen Energy 33 (2008) 2337–2354.
[19] A. Brisse, J. Schefold, M. Zahid, Int. J. Hydrogen Energy 33 (2008) 5375–5382.
[20] D. Pletcher, X. Li, Int. J. Hydrogen Energy 36 (2011) 15089–15104.
[21] X. Wu, K. Scott, J. Power Sources 206 (2012) 14–19.
[22] X. Wu, K. Scott, Int. J. Hydrogen Energy 38 (2013) 3123–3129.
[23] M. Santarelli, P. Medina, M. Calì, Int. J. Hydrogen Energy 34 (2009) 2519–2530.

[24] P. Millet, D. Dragoe, S. Grigoriev, V. Fateev, C. Etievant, Int. J. Hydrogen Energy 34 (2009) 4974–4982.
[25] P. Millet, R. Ngameni, S.A. Grigoriev, N. Mbemba, F. Brisset, A. Ranjbari, C. Etiévant, Int. J. Hydrogen Energy 35 (2010) 5043–5052.
[26] J.C. Cruz, V. Baglio, S. Siracusano, V. Antonucci, A.S. Aricò, R. Ornelas, L. Ortiz-Frade, G. Osorio-Monreal, S.M. Durón-Torres, L.G. Arriaga, Int. J. Electrochem. Sci. 6 (2011) 6607–6619.
[27] Y. Lee, H.-Y. Shin, S.H. Chun, J. Lee, W.J. Park, J.M. Baik, S. Yoon, M.H. Kim, J. Phys. Chem. C 116 (2012) 16300–16304.
[28] J.C. Cruz, V. Baglio, S. Siracusano, R. Ornelas, L. Ortiz-Frade, L.G. Arriaga, V. Antonucci, A.S. Aricò, J. Nanopart. Res. 13 (2011) 1639–1646.
[29] O.I. Velikokhatnyi, K. Kadakia, K. Moni, M.K. Datta, P.N. Kumta, J. Phys. Chem. C 117 (2013) 20542–20547.
[30] S. Siracusano, V. Baglio, A. Stassi, R. Ornelas, V. Antonucci, A.S. Arico, Int. J. Hydrogen Energy 36 (2011) 7822–7831.
[31] F. Bonet, V. Delmas, S. Grugeon, R. Herrera-Urbina, P. Silvert, K. Tekaia-Elhsissen, Nanostruct. Mater. 11 (1999) 1277–1284.
[32] L. Kurihara, G. Chow, P. Schoen, Nanostruct. Mater. 5 (1995) 607–613.
[33] Y. Murakami, H. Ohkawauchi, M. Ito, K. Yahikozawa, Y. Takasu, Electrochim. Acta 39 (1994) 2551–2554.
[34] Y. Murakami, S. Tsuchiya, K. Yahikozawa, Y. Takasu, Electrochim. Acta 39 (1994) 651–654.
[35] M. Ito, Y. Murakami, H. Kaji, H. Ohawauchi, K. Yahikozawa, Y. Takasu, J. Electrochem. Soc. 141 (1994) 1242–1245.
[36] K. Kameyama, S. Shohji, S. Onoue, K. Nishimura, K. Yahikozawa, Y. Takasu, J. Electrochem. Soc. 140 (1993) 1036–1037.
[37] T. Lassali, J. Boodts, L. Bulhoes, J. Non-Cryst. Solids 273 (2000) 129–134.
[38] A. Marshall, B. Børresen, G. Hagenm, M. Tsypkin, R. Tunold, Mater. Chem. Phys. 94 (2005) 226–232.
[39] R. Adams, R.L. Shriner, J. Am. Chem. Soc. 45 (1923) 2171–2179.
[40] E. Rasten, Electrocatalysis in water electrolysis with solid polymer electrolyte (Ph.D. thesis), NTNU, Trondheim, Norway, 2001.
[41] E. Rasten, G. Hagen, R. Tunold, Electrochemical Society Proceedings, Pennington, 1991, p. 151.
[42] A. Marshall, B. Børresen, G. Hagen, M. Tsypkin, R. Tunold, First European hydrogen energy conference 2–5 September, Grenoble, France CO1/71, 2003.
[43] R. Hutchings, K. Muller, S. Stucki, J. Mater. Sci. 19 (1984) 3987–3994.
[44] S. Song, H. Zhang, X. Ma, Z. Shao, R.T. Baker, B. Yi, Int. J. Hydrogen Energy 33 (2008) 4955–4961.
[45] A.S. Aricò, A. Stassi, E. Modica, R. Ornelas, I. Gatto, E. Passalacqua, V. Antonucci, J. Power Sources 178 (2008) 525–536.
[46] C. Angelietta, S. Trasatti, L.D. Atanasoska, R.T. Atanasoski, J. Electroanal. Chem. 214 (1986) 535–546.
[47] C. Angelietta, S. Trasatti, Mater. Chem. Phys. 22 (1989) 231–247.
[48] K. Kameyama, K. Tsukada, K. Yahikozawa, Y. Takasu, J. Electrochem. Soc. 141 (1994) 643–647.
[49] L.E. Owe, M. Tsypkin, K.S. Wallwork, R.G. Haverkamp, S. Sunde, Electrochim. Acta 70 (2012) 158–164.
[50] A. De Battisti, G. Lodi, M. Cappadonia, G. Battaglin, R. Kötz, J. Electrochem. Soc. 136 (1989) 2596–2598.
[51] R. Kötz, S. Stucki, Electrochim. Acta 31 (1986) 1311–1316.
[52] T.J. Kemp (Ed.), Instrumental methods in electrochemistry. Ellis Horwood series in Physical Chemistry, Southampton Electrochemistry Group, University of Southampton, 1985, pp. 1–443.
[53] S. Trasatti, Electrochim. Acta 36 (1991) 225–241.
[54] J. Rossmeisl, Z.W. Qu, H. Zhu, G.J. Kroes, J.K. Nørskov, J. Electroanal. Chem. 607 (2007) 83–89.
[55] A.S. Aricò, S. Srinivasan, V. Antonucci, Fuel Cells 1 (2001) 133–161.
[56] S. Trasatti, Electrochim. Acta 29 (1984) 1503–1512.
[57] A.T. Marshall, S. Sunde, M. Tsypkin, R. Tunold, Int. J. Hydrogen Energy 32 (2007) 2320–2324.
[58] J. Cheng, H. Zhang, G. Chen, Y. Zhang, Electrochim. Acta 54 (2009) 6250–6256.
[59] E. Mayousse, F. Maillard, F. Fouda-Onana, O. Sicardy, N. Guillet, Int. J. Hydrogen Energy 36 (2011) 10474–10481.
[60] N. Mamaca, E. Mayousse, S. Arrii-Clacens, T.W. Napporn, K. Servat, N. Guillet, K.B. Kokoh, Appl. Catal. B: Environ. 111–112 (2012) 376–380.
[61] G. Li, H. Yu, W. Song, X. Wanga, Y. Li, Z. Shao, B. Yi, Int. J. Hydrogen Energy 37 (2012) 16786–16794.